JMEPEG (2010) 19:99–106
DOI: 10.1007/s11665-009-9439-1

1059-9495/$19.00

Fatigue Crack Growth of Peened Friction Stir-Welded 7075 Aluminum Alloy under Different Load Ratios

Omar Hatamleh, Scott Forth, and Anthony P. Reynolds

(Submitted April 8, 2008; in revised form March 16, 2009)

The effect of peening on the fatigue crack growth performance of friction stir-welded 7075 aluminum alloy was investigated. The fatigue crack growth rates were assessed for laser- and shot-peening conditions at stress ratios (*R*) of 0.1 and 0.7. The surface and through thickness residual stress distributions were characterized for the different regions in the weld. The results indicate a significant reduction in fatigue crack growth rates using laser peening compared to shot peening and the as-welded condition. The effect of the compressive stresses obtained through laser peening was deemed responsible for increasing the resistance to fatigue crack growth of the welds.

Keywords fatigue crack growth, friction stir welding, laser peening, shot peening, stress ratio, 7075

1. Introduction

High-strength aluminum alloys, such as 7075-T7351, are commonly used in the aerospace industry because of their attractive properties. Unfortunately, these aluminum alloys are difficult to weld using conventional fusion welding, and therefore are mechanically joined at higher cost. The difficulty in welding aluminum structure is due to the mechanical properties of the welded joints being degraded because of the dendritic structure formed during the fusion welding process (Ref 1, 2).

Friction stir welding (FSW) was invented by the Welding Institute in England (Ref 3) and is currently being targeted for structurally demanding applications. Since its invention in 1991, FSW has emerged as a promising solid state joining process capable of producing high-quality joints in high-strength aluminum alloys. This technique transforms metals into a plastic state at a temperature below the melting temperature of the material (Ref 4, 5), and then mechanically stirs the materials together under pressure to form a high-strength welded joint. FSW is considered a solid state welding process; therefore, the heat affected zone (HAZ) size and microstructure, and residual stress fields around the weld, are different from those produced using conventional fusion welding (Ref 6). The FSW consists of a nugget, or stirred zone, the thermo-mechanical affected zone (TMAZ), and a HAZ.

Omar Hatamleh, Structures Branch, NASA–Johnson Space Center, Houston, TX 77058; **Scott Forth**, Materials Branch, NASA–Johnson Space Center, Houston, TX 77058; and **Anthony P. Reynolds**, Mechanical Engineering Department, University of South Carolina, Columbia, SC 29208. Contact e-mail: omar.hatamleh-1@nasa.gov.

Surface tensile residual stresses that may develop as a result of welding can significantly degrade the performance of the welds with regards to fatigue properties. Therefore, introducing a layer of compressive residual stress on the surface may extend the fatigue life by delaying the crack initiation and propagation. Surface processing techniques like shot peening and laser peening (LP) are capable of generating compressive residual stresses on the surface. These compressive residual stresses can moderate the surface tensile residual stresses produced during welding. Shot peening introduces multiple overlapping impacts using glass or metal spheres to introduce a layer of compressive stress, while LP uses high-energy laser pulses (several GW/cm^2) at the surface of metals.

A previous study by Hatamleh et al. (Ref 7) investigated the fatigue crack growth in a 0.625-cm-thick peened FSW 7075-T651 at a stress ratio of $R = 0.1$. The results indicated a significant decrease in fatigue crack growth rates (FCGR) resulting from using LP compared with native welded and unwelded specimens. In this investigation, the work is expanded to explore the peening effect on thicker (1.25 cm) FSW plates. The effects of the residual stresses resulting from laser and shot peening on FCGR will also include low (0.1) and high (0.7) stress ratios. In addition, the surface and subsurface residual stresses were assessed for all the conditions investigated, and the effect of the different processing conditions on crack initiation was also assessed.

2. Experimental Setup

A 7075-T651 aluminum alloy plate with a thickness of 1.25 cm was used in this investigation. The 7xxx series alloys are well suited for many aerospace applications due to their high strength and acceptable corrosion resistance. For the FSW process, a tool with a shoulder diameter of 3.3 cm and probe diameter of 0.92 cm was used. The rotational speed consisted of 300 rpm in the counterclockwise direction with a translation speed of 15 cm/min. The welding direction was aligned with the material rolling direction, and the dimensions of the FSW panels were 91 cm × 30 cm × 1.25 cm. Following the welding

process, the AA 7075 welded plates were aged from the T651 condition to the T7351 in accordance with SAE AMS-H-6088 requirements. The FSW puts the weld nugget microstructure in a supersaturated solid solution condition; therefore, heat treatment is necessary to prevent the welded material from continuing to age at room temperature (Ref 8, 9). In order to evaluate the quality of the weld, bending tests using strip specimens were performed on both the root and the crown sides of the weld. The microstructure of the weld zone was assessed using optical and scanning electron microscopes.

In this study, middle through crack tension, M(T), specimens with dimensions in accordance with ASTM E647 were cut from the welded plates as shown in Fig. 1. The crack in the specimens was perpendicular to the weld line and centered in the weld nugget. Fatigue crack growth specimens consisted of unpeened, shot-peened, and laser-peened welded specimens. The shot-peening process was performed at an Almen intensity of 0.008-0.012 A, while LP was processed using a laser power density of 5 GW/cm^2 and 18 ns in duration. Three layers of LP were applied on each of the laser-peened specimens.

The global mechanical properties of the welded plates were tested using transverse tensile specimens that consisted of

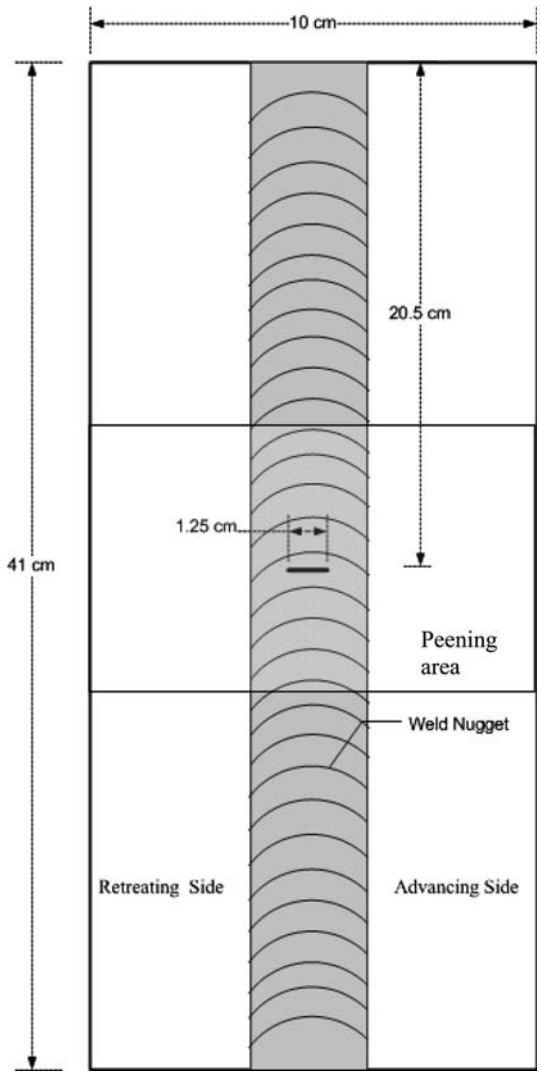

Fig. 1 Fatigue crack growth specimen

conventional dog bone coupons that were 20 cm long with a gage length of 8.5 cm and a gage width of 1.25 cm. The weld was in the center of the specimen and the load was applied perpendicular to the weld direction. The local tensile properties in the weld were measured using a digital image correlation technique through an ARAMIS system (Ref 10, 11). The strain is measured using a three-dimensional video correlation method and high-resolution digital cameras assuming an iso-stress condition. The iso-stress assumption suggests that the different regions of the weld are arranged in series and that the cross section at any location in the specimen is homogeneous (Ref 12, 13). Therefore, this assumption implies that the stress is uniform over the cross section and is equal to the average stress. The accuracy of the measured tensile properties is therefore determined by the degree of non-homogeneity at all cross sections to which the load is applied.

The x-ray diffraction (XRD) and contour methods were utilized to measure the residual stresses in the samples. In XRD, the strain in the crystal lattice was measured, and the residual stresses inducing the strain were calculated assuming that the crystal lattice is linearly distorted. Residual stresses were measured in both the transverse and the longitudinal directions at different locations across the weld as illustrated in Fig. 2. The locations corresponded to the weld centerline, weld interface, the HAZ, and base material. The residual stress measurements were taken using 3- and 1-mm-diameter collimators. The small size beam was used to measure stresses in the weld nugget since the grain size in that region is fine and equiaxed. The larger collimator was used to measure the stresses in the HAZ because of the larger grain size in that region. A larger collimator can collect a larger sample size reducing scatter and resulting in higher precision at the cost of reduced spatial resolution. All the measurements obtained through XRD were surface measurements (up to 0.012 mm from the surface). The XRD was performed through a Proto Manufacturing laboratory x-ray diffraction system using Cr target x-ray tube energized at 25 kV and 7 mA.

To determine the residual stresses using the contour method, the specimens were cut along the measurement plane outlined in Fig. 2 with an EDM wire. The deformed surface shape resulting from the relaxed residual stresses was measured on both cutting surfaces using a coordinate measuring machine (CMM) with a tolerance of 0.0025 mm. The displacements from both cutting surfaces were then averaged, and the noise in the measurements was filtered from average displacements by fitting to a smooth analytical surface. Since the contour is uniquely related to the original residual stresses, the residual stresses were calculated directly using a finite element model (FEM). A 3-D model of the FSW specimen after it has been cut is constructed, and starting from a flat surface, the displacement boundary conditions are used to force the cut surface to the opposite of the measured surface contour. This is then used to extract the residual stresses normal to the surface (Ref 14, 15).

After the peening process, a 0.25-mm-thick through the thickness starter crack was produced in each of the fatigue testing specimens using an electric discharge machine (EDM). The fatigue testing was performed under axial loading using a servo-hydraulic machine. The fatigue crack growth rates (FCGR) measurements were carried out at constant amplitude loads in laboratory air at stress ratios, R, of 0.1 and 0.7. The number of samples used in the testing is outlined in Table 1.

Prior to conducting the FCGR tests, the specimens were cycled until a precrack measuring 0.5 mm was obtained from

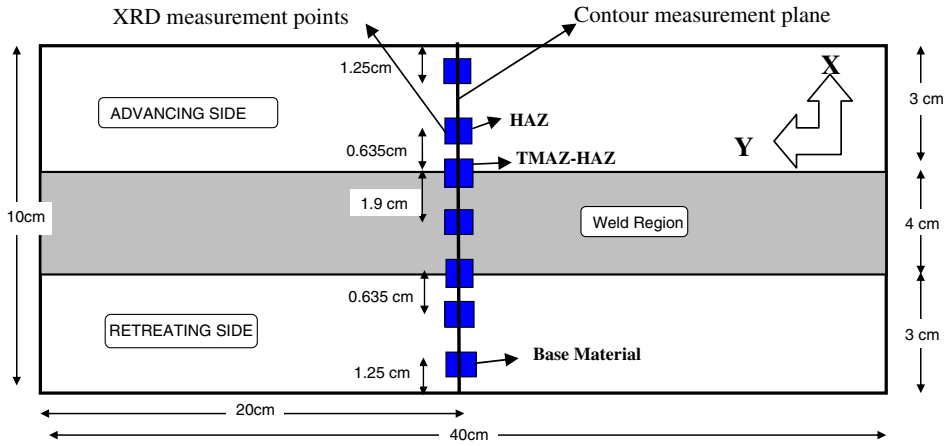

Fig. 2 Locations of residual stress measurements

Table 1 Number of samples tested

	Base material	As-welded	Shot peening	Laser peening
$R = 0.1$	1 sample	2 samples	2 samples	2 samples
$R = 0.7$	1 sample	2 samples	2 samples	2 samples

both sides of the EDM notch. The fatigue behavior in the tests was determined by measuring the fatigue crack length (a) versus the number of cycles (N). The FCGR tests were performed on four conditions: parent material, welded plates, and welded plates with either shot or laser peening.

3. Results and Discussion

3.1 Weld Microstructure

A metallographic cross section of the 7075 FSW is shown in Fig. 3. The metallographic section shows a classic weld nugget region and the stirring marks, commonly denoted as "onion rings," typically found in this region of the weld. The difference in contrast between the onion rings is not due to variations in grain size or particle density, which implies that the onion rings structure in this alloy may be formed by texture variations (Ref 16, 17). The FSW samples showed no evidence of defects. The weld nugget is wider on the crown region of the weld because the upper surface of the weld contacts with the tool shoulder and the probe is tapered (8°).

The structure at the nugget is fine and equiaxed with grain sizes significantly smaller than the parent material grain due to the higher temperature and extensive plastic deformation. The average grain size in the nugget was measured using ASTM E-112 standard and was approximately 5 μm. Several recent papers have also investigated the microstructure resulting from FSW on AA 7075-T6 (Ref 2, 9, 18, 19), and indicated a fine equiaxed grain structure in the weld nugget of approximately 3-10 μm.

The grain structure at the TMAZ region was elongated with some considerable distortions due to the mechanical action from the welding tool. The HAZ is unaffected by the mechanical effects from the welding tool, and the grain structure in that region resembles the parent material grain structure.

3.2 Mechanical Properties and Hardness

To assess the hardness and strength distribution across the weld region, microhardness measurements were taken as shown in Fig. 4. The weld region exhibits the "W"-shaped hardness distribution which is typical of many friction stir welds in precipitation hardening alloys. The hardness minima in the advancing and retreating side HAZs are a result of peak temperatures in those regions being optimum for precipitate coarsening. The recovery (to nearly base metal values) of hardness in the weld nugget is due to the attainment of near solution heat-treatment temperature in that part of the weld. Hence, significant solute is available for re-precipitation during post-weld aging treatment (Ref 20). Tensile test results are shown in Fig. 5. The fracture locations were at or near the interface between the weld nugget and the TMAZ at a 45° angle on the retreating side. The interface between the weld nugget and TMAZ correspond to a low hardness area because the original structure in this region is over aged. Therefore, this area of the weld will be relatively ineffective in inhibiting dislocation motion and the strain localization in the softened area of the weld will result in a reduction in overall elongation in transverse tension. The consistent failure at the retreating side also suggests that the tensile properties of the welded joint are not symmetric on the two interfaces of the weld, and that the tensile properties on the retreating side are weaker than the advancing side. All properties for the welded specimens were lower than for the base unwelded material.

3.3 Residual Stress

The surface longitudinal and transverse residual stresses measured by XRD for the different samples are shown in Fig. 6 and 7, respectively. The highest magnitude residual stresses were measured at or near the edge of the tool shoulder near the TMAZ. Several researchers (Ref 16, 21) have also reported that the transition between the nugget and the TMAZ had localized residual stresses higher than other areas of the weld. The original surface residual stresses on the large FSW plate were probably reduced after the heat treatment following the welding process. In addition, residual stress relaxation may have resulted from sectioning the specimens from the large welded plates. Therefore, the residual stress values shown in Fig. 6 and 7 may be less than the original stresses found on the large welded plate.

Fig. 3 Metallographic cross section of 7075 friction stir weld

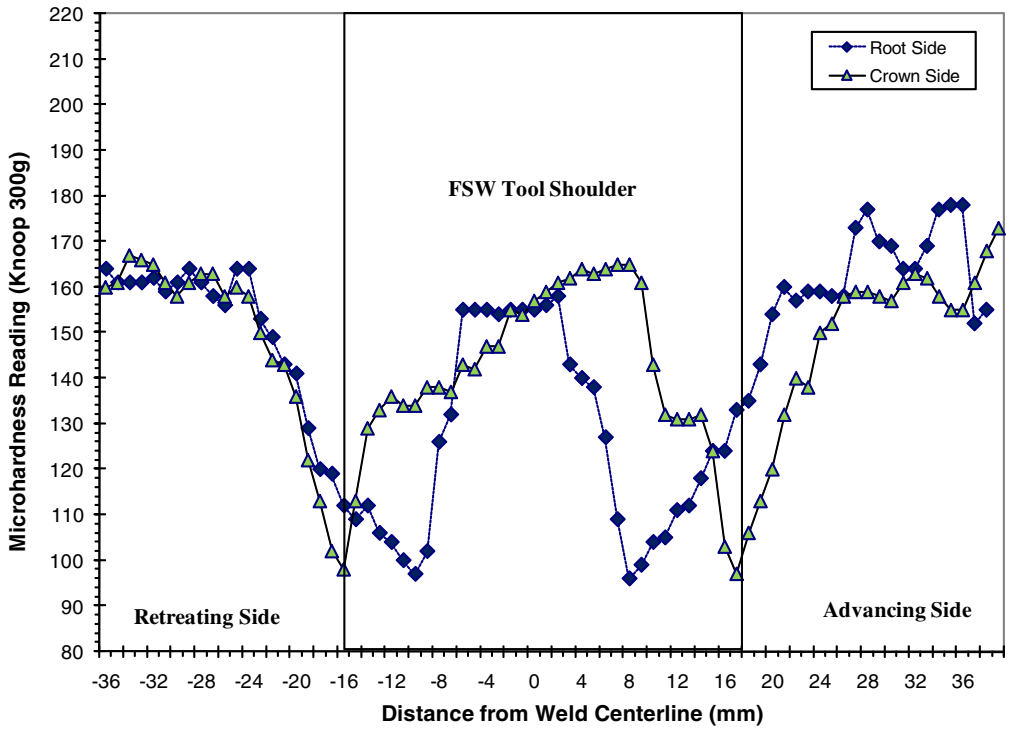

Fig. 4 The microhardness profile across the weld region for FSW 7075

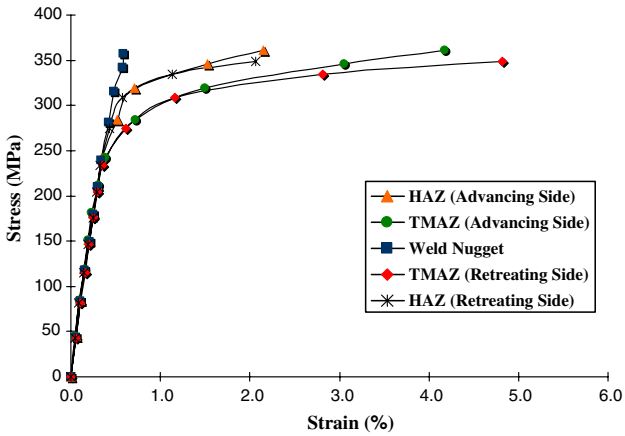

Fig. 5 Tensile properties at different regions of the weld for FSW 7075

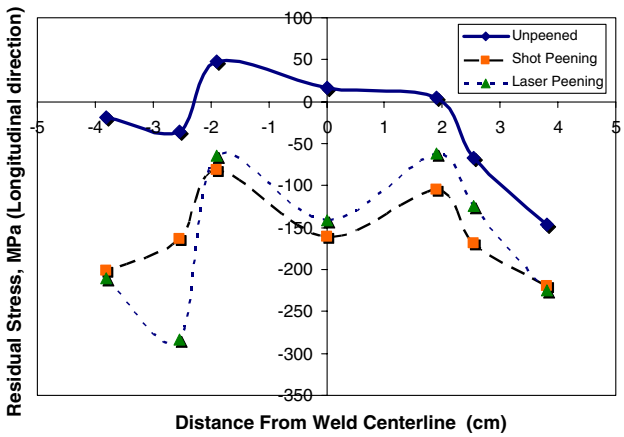

Fig. 6 Surface residual stresses for the various peened FSW specimens (longitudinal)

Shot and laser peening of the sectioned samples had a more symmetric residual stress profile across the weld. The shot peening led to a relatively higher and more uniform surface residual stress field, due to the high amount of cold work associated with shot peening. Conversely, LP had little effect on the residual stresses at the edge of the weld in the TMAZ

region in the transverse direction. That location happened to coincide with the lowest hardness point outlined in Fig. 4. Hatamleh (Ref 22) investigated the effects of peening on the hardness changes in FSW AA 7075. In that investigation, laser peening FSW AA 7075 resulted in an increase in hardness across the weld region. Moreover, the increases at the edges of the weld nugget/TMAZ where the material had its lowest hardness levels did not improve by an appreciable amount. The nature of the metallurgical state in that region will eventually result in a saturation of the surface hardening and suggests there is a limit to hardness increase due to LP.

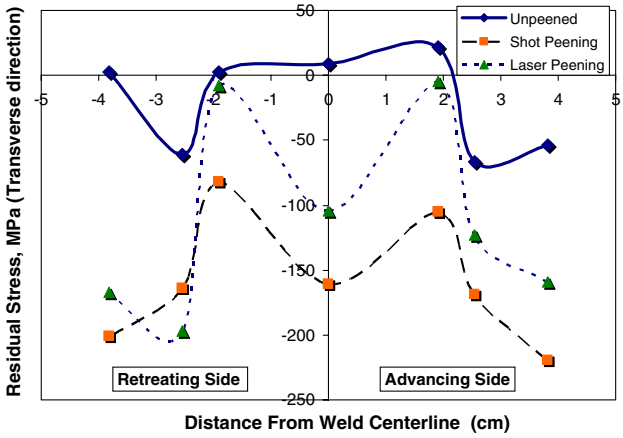

Fig. 7 Surface residual stresses for the various peened FSW specimens (transverse)

The contour plots illustrating the measured through thickness residual stresses determined by the contour method are shown in Fig. 8-10. Overall, the shot-peened coupons exhibited only slight variation in through thickness residual stresses compared to the unpeened FSW coupons. The main difference was noticed near the coupon surfaces where shot peening produces a localized area of compressive residual stress. LP, on the other hand, produced very significant levels of compressive residual stress near the surface. These residual stresses had a drastic effect on the overall residual stress state and produced significant levels of sub-surface compensating tensile residual stress that extended to the specimen edges. It is interesting to note that the weld-induced residual stresses in the TMAZ/HAZ are greatly reduced by the laser-peening process; however, the compressive residual stress due to LP is less in the surfaces corresponding to the HAZ/TMAZ region. Therefore, these results outline the necessity to obtain full thickness measurements in order to obtain a clear picture of the residuals stress state in the welds.

3.3.1 FSW Specimen. The bulk residual stress data obtained using the contour method show that LP has a varying effect on residual stress across the weld. To further illustrate this effect, the net change in residual stress from LP was calculated across the width of the coupon at a depth of 1 mm below the top surface. That calculation was performed by subtracting the residual stress in the unpeened coupon from the residual stress in the laser-peened coupons. It can be seen from

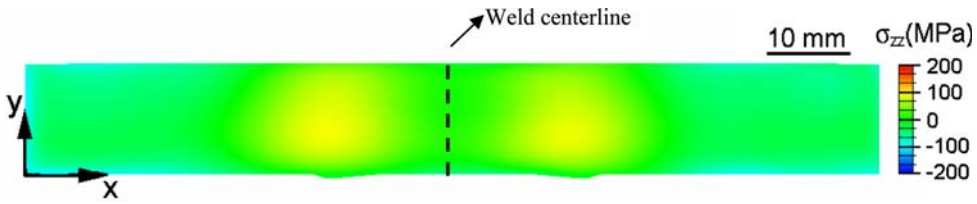

Fig. 8 Two-dimensional map of the measured residual stress for the unpeened FSW specimen

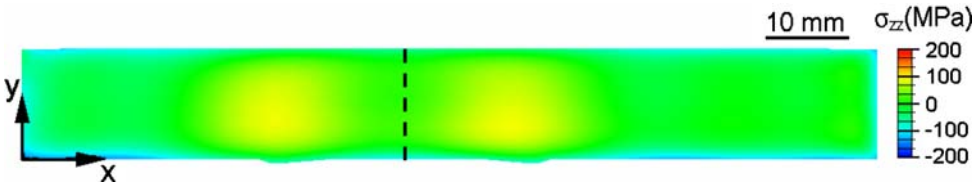

Fig. 9 Two-dimensional map of the measured residual stress for the shot-peened FSW specimen

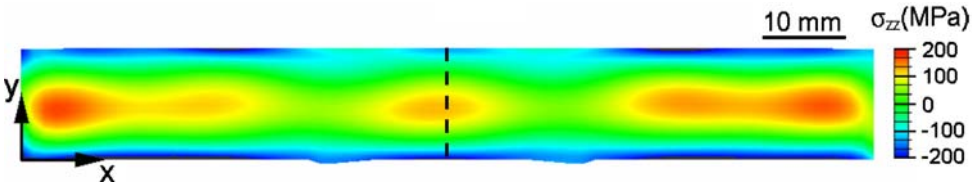

Fig. 10 Two-dimensional map of the measured residual stress for the laser-peened FSW specimen

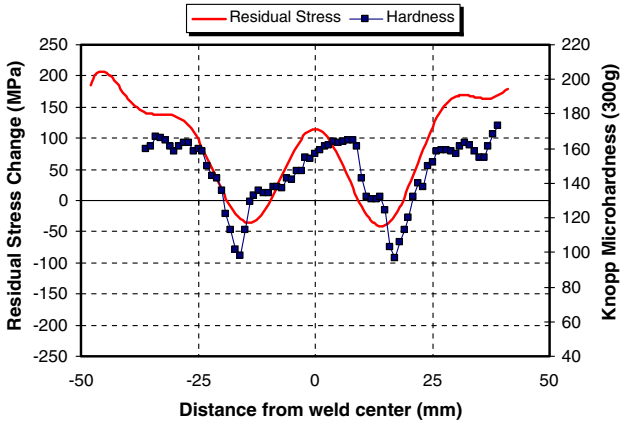

Fig. 11 Residual stress values from laser peening compared with the hardness measurements for FSW specimen

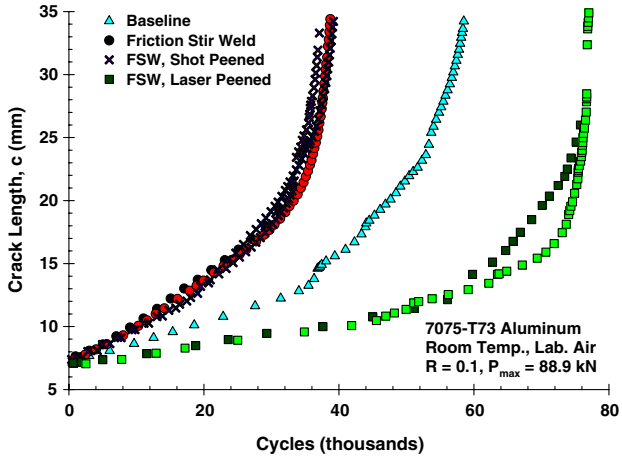

Fig. 12 Crack length vs. cycles, $R = 0.1$ (different colors of the same legend represent different samples used)

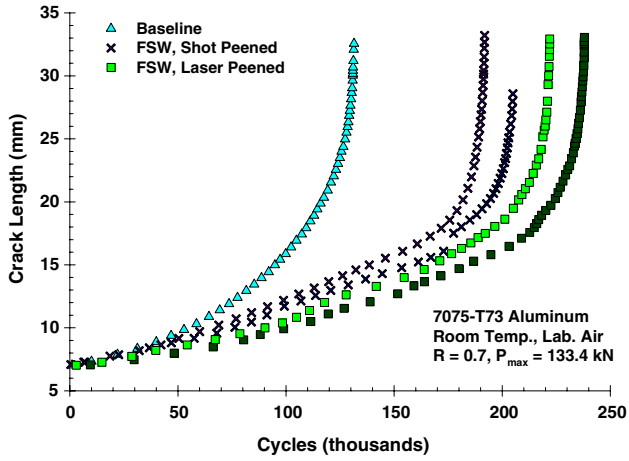

Fig. 13 Crack length vs. cycles, $R = 0.7$ (different colors of the same legend represent different samples used)

Fig. 11 that there exist a strong correlation between the hardness levels and the residual stresses in the laser-peened sample. Since the amount of residual stress is limited by the yield strength of the material, it is expected that LP will have limited effect on the regions of low hardness.

3.4 Fatigue Crack Propagation

Fatigue crack growth rate testing was performed on M(T) specimens as described in the "Experimental procedures" section. Tests were conducted such that the crack would propagate transverse to the weld and therefore grow through the nugget, TMAZ, HAZ, and finally into the parent material. Testing was performed under constant load amplitude at a frequency of 22 Hz. Figure 12 shows a plot of crack length measured at the surface of the specimens to cycle count for testing performed at a stress ratio, R, of 0.1 on the base material and with the FSW in both the unpeened and peened conditions.

The FSW crack growth rate (circles) is accelerated compared to the parent material (triangles). This behavior may be attributed to the tensile residual stresses measured in the weld (Fig. 6-8) which are accelerating the crack growth. John et al. (Ref 8) investigated the fatigue crack growth behavior in friction stir welds, and indicated that the difference in FCG between the FSW and the base material was due to the contribution from the residual stresses, and not the microstructure. Another recent study by Pouget and Reynolds (Ref 23) also demonstrated that fatigue crack propagation in friction stir-welded 2050 was strongly dependent on the presence of residual stresses. However, they also indicated that other factors such as microstructure and closure effects resulting from sources other than residual stresses must be accounted for.

Shot peening over the FSW (X's) does not appear to affect the crack growth response of the FSW samples (circles). This lack of an effect is surprising, considering high-surface compressive residual stresses were measured in the shot-peened samples (Fig. 6 and 7). However, the measured through thickness residual stresses imparted from shot peening were similar to the FSW process in Fig. 8 and 9. It would appear in the case of the $R = 0.1$ testing that the shot peening had little affect, as noted in the crack growth testing. In contrast to the shot-peening results, the laser-peened FSW specimens have the expected retarded crack growth rate due to the compressive residual stresses (Fig. 6, 7, and 10).

Figure 13 shows a plot of crack length versus cycles for a stress ratio of 0.7. The data are similar to the $R = 0.1$ data presented in Fig. 12, with the exception of the unpeened friction stir-welded condition. The unpeened FSW case was tested with a maximum load of 115.6 kN, and the crack length versus cycles behavior cannot be plotted on the same figure as data generated with a maximum load of 133.4 kN. However, all the data can be plotted as crack growth rate, da/dN, versus stress the applied intensity factor range, $\Delta K_{applied}$, as shown in Fig. 14. Since all of the testing was performed at constant load amplitudes, the plots of crack length versus cycle count and crack growth rate versus stress intensity are directly relatable, e.g. the data in the lower left of Fig. 14 are computed from the data in the lower left of Fig. 13.

Investigating the data, there are several differences between the $R = 0.1$ and 0.7 data. First, the unpeened friction stir-welded specimens propagated at a faster and slower rate than the base material at $R = 0.1$ and 0.7, respectively. The effect of a residual stress, which affects mean stress, should be minimal at high values of R because the applied mean stress increases as R increases, and therefore the residual stress becomes a smaller portion of the total mean stress. The retardation of the $R = 0.7$

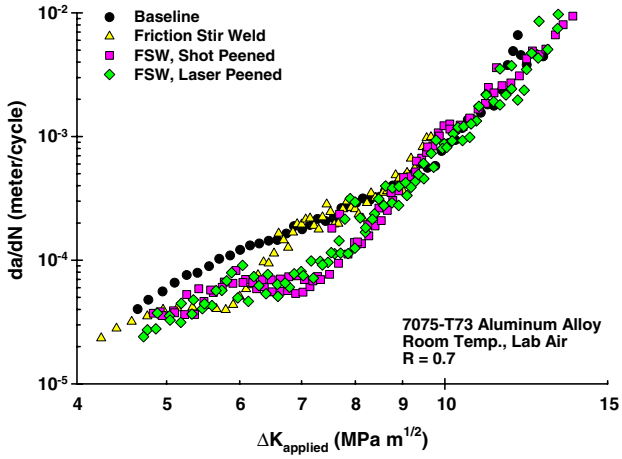

Fig. 14 Crack growth rate vs. applied stress intensity factor range, $R = 0.7$, for base, friction stir-welded and peened aluminum

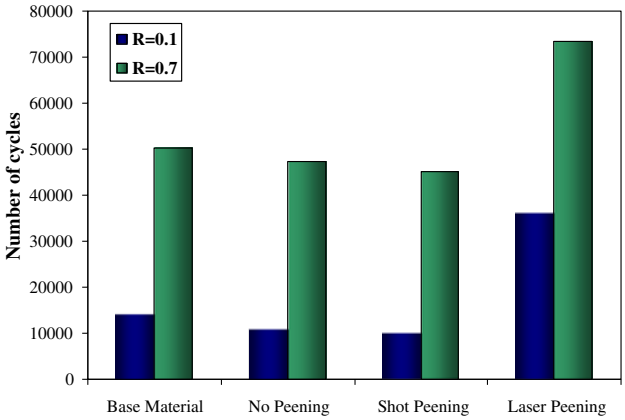

Fig. 15 Number of cycles to precrack a 0.5-mm-long crack from the starter notch on the FSW joint

unpeened friction stir-weld data, opposite of what was observed in the $R = 0.1$ data, is counter-intuitive due to the measured tensile residual stresses (Fig. 7 and 8). Second, the lack of an affect of the shot-peening compressive residual stresses at $R = 0.1$ stress ratio is puzzling. The residual stresses measured using XRD showed compressive stresses (Fig. 6 and 7), whereas the contour method showed no effect (Fig. 9). Based on the crack growth testing, it would appear that the shot-peening residual stress field is negligible when compared to the as-welded condition, as shown in Fig. 12 and 14. This would imply that the contour method is more accurate than XRD in measuring the residual stresses that affect crack growth. Finally, the laser shot peening behaved as expected and consistently retarded crack growth.

Figure 15 outlines the number of cycles required to pre-crack a 0.5-mm-long crack from one side of the EDM starter notch for the different processed samples. The results are outlined in terms of two R ratios ($R = 0.1$ and 0.7). The specimens processed with shot peening had no improvement when compared to the unpeened specimens. The laser-peened samples, on the other hand, demonstrated substantial reduction in fatigue crack growth even when compared to the base unwelded material. For examples for the case of $R = 0.1$, it took three times the number of cycles to grow the 0.5 mm when compared to the unpeened FSW sample. The result for the reduction in crack growth was evident at both R ratios.

4. Conclusions

The influence of laser and shot peening on the fatigue crack growth performance of friction stir-welded 7075-T7351 aluminum alloy was investigated at high- and low-stress ratios. Residual stresses were measured on the samples prior to testing. Both surface and through thickness residual stress distributions were investigated and characterized for the various regions in the weld.

1. Through thickness residual stress measurements indicate that LP introduced higher and deeper compressive stresses compared to the shot peening.
2. The crack growth results indicate that residual stresses play a key role in the crack growth. The residual stresses from FSW caused both acceleration and retardation of the cracks.
3. Shot peening of the friction stir-welded specimens had little effect on FCGR.
4. There exist a strong correlation between the hardness levels and the residual stresses in the laser-peened sample.
5. The number of cycles to crack initiation was increased for LP over shot peening and as-welded condition by a factor of approximately three for $R = 0.1$ and a factor of approximately two for $R = 0.7$
6. A significant difference was obtained in crack extension rate at $R = 0.1$ between laser- and shot-peened samples with laser-peened sample crack growth much slower than the shot-peened samples. That difference was reduced for the $R = 0.7$ case.

References

1. P. Pao, S. Gill, C. Feng, and K. Sankaran, Corrosion-Fatigue Crack Growth in Friction Stir Welded Al 7075, *Scr. Mater.*, 2001, **45**, p 605–612
2. C. Rhodes, M. Mahoney, W. Bingel, R. Spurling, and W. Bampton, Effects of Friction Stir Welding on Microstructure of 7075 Aluminum, *Scr. Mater.*, 1997, **36**(1), p 69–75
3. W.M. Thomas, E.D. Nicholas, J.C. Needham, M.G. Murch, P. Templesmith, and C.J. Dawes, Friction Stir Butt Welding, Int Patent App PCT/GB92/02203, and GB Patent App 9125978.8, 297 US patent No. 5,460,317, October 1995
4. P. Staron, M. Kocak, S. Williams, and A. Wescott, Residual Stress in Friction Stir-Welded A1 Sheets, *Phys. B: Condens. Matter*, 2004, **350**(Suppl 1–3), p e491–e493
5. M. Ericsson and R. Sandstrom, Influence of Welding Speed on the Fatigue of Friction Stir Welds, and Comparison with MIG and TIG, *Int. J. Fatigue*, 2003, **25**, p 1379–1387
6. G. Bussu and P.E. Irving, The Role of Residual Stress and Heat Affected Zone Properties on Fatigue Crack Propagation in Friction Stir Welded 2024-T351 Aluminum Joints, *Int. J. Fatigue*, 2003, **25**, p 77–88
7. O. Hatamleh, J. Lyons, and R. Forman, Laser and Shot Peening Effects on Fatigue Crack Growth in Friction Stir Welded 7075-T7351 Aluminum Alloy Joints, *Int. J. Fatigue*, 2007, **29**(3), p 421–434
8. R. John, et al., Residual Stress Effects on Near-Threshold Fatigue Crack Growth in Friction Stir Welds in Aerospace Alloys, *Int. J. Fatigue*, 2003, **25**, p 939–948

9. M.W. Mahoney, Properties of Friction-Stir-Welded 7075 T651 Aluminum, *Metall. Mater. Trans. A*, 1998, **29**, p 1955–1964
10. J. Tyson, T. Schmidt, and K. Galanulis, Advanced Photogrammetry for Robust Deformation and Strain Measurement, *Proceedings of SEM 2002 Annual Conference* (Milwaukee, WI), June 2002
11. T. Schmidt, J. Tyson, and K. Galanulis, Full-Field Dynamic Displacement and Strain Measurement Using Advanced 3D Image Correlation Photogrammetry, *Exp. Tech.*, 2003, **27**(3), p 41–44
12. W.D. Lockwood, B. Tomas, and A.P. Reynolds, Mechanical Response of Friction Stir Welded AA 2024: Experiment and Modeling, *Mater. Sci. Eng. A*, 2002, **323**(1–2), p 349–354
13. W.D. Lockwood and A.P. Reynolds, Simulation of the Global Response of a Friction Stir Weld Using Local Constitutive Behavior, *Mater. Sci. Eng. A*, 2003, **339**(1–2), p 35–42
14. M. Prime and A.R. Gonzales, The Contour Method: Simple 2-D Mapping of Residual Stresses, *Proceedings of the 6th International Conference on Residual Stresses*, Vol. 1 (Oxford, UK), July 10–12, 2000, p 617–624
15. M. Prime, Cross-Sectional Mapping of Residual Stresses by Measuring the Surface Contour After a Cut, *J. Eng. Mater. Technol.*, 2001, **123**, p 162–168
16. M. Peel, et al., Microstructure, Mechanical Properties and Residual Stresses as a Function of Welding Speed in Aluminum AA5083 Friction Stir Welds, *Acta Mater.*, 2003, **51**, p 4791–4801
17. L. Svenson, L. Karlsson, H. Larsson, B. Karlsson, M. Fazzini, and J. Karlsson, Microstructure and Mechanical Properties of Friction Stir Welded Aluminium Alloys with Special Reference to AA 5083 and AA 6082, *Sci. Technol. Weld. Join.*, 2000, **5**(5), p 285–296
18. A. Goloborodko, et al., Friction Stir Welding of a Commercial 7075-T6 Aluminum Alloy: Grain Refinement, Thermal Stability and Tensile Properties, *Mater. Trans.*, 2004, **45**(8), p 2503–2508
19. T. Venugopal, et al., Studies on Friction Stir Welded AA 7075 Aluminum Alloy, *Trans. Indian Inst. Met.*, 2004, **57**(6), p 659–663
20. A.P. Reynolds, W. Tang, Z. Khandkar, J.A. Khan, and K. Lindner, Relationships Among Weld Parameters, Hardness Distributions, Temperature Histories in Alloy 7050 Friction Stir Welds, *Sci. Technol. Weld. Join.*, 2005, **10**(2), p 190–199
21. C. Dale Donne, E. Lima, J. Wegener, A. Pyzalla, and T. Buslaps, Investigations on Residual Stresses in Friction Stir Welds, *3rd International Symposium on Friction Stir Welding* (Kobe, Japan), 2001
22. O. Hatamleh, Surface Hardness Changes in Laser Peened Friction Stir Welded 2195 and 7075 Aluminum Alloys, *Int. J. Surf. Sci. Eng.*, 2008, **2**(1/2)
23. G. Pouget and A.P. Reynolds, Residual Stress and Microstructure Effects on Fatigue Crack Growth in AA2050 Friction Stir Welds, *Int. J. Fatigue*, 2008, **30**, p 463–472